Synthesis, spectroscopic characterization, DFT, oxygen binding and antioxidant activity of Fe(III), Co(II) and Ni(II) complexes with a tetradentate ONNO donor Schiff base ligand

SATYENDRA N. SHUKLA*, PRATIKSHA GAUR, MOHAN L. RAIDAS
and SANJAY S. BAGRI

Coordination Chemistry Research Lab, Department of Chemistry, Govt. Science College, Jabalpur (M.P.), India

Abstract: The Schiff base ligand, namely (7*E*)-*N*-benzylidene-2-styrylbenzen-amine-1,2-diamine-2,4-dihydroxy-phenol (**L**), was synthesized by conden-sation of 2,4-dihydroxybenzaldehyde with *o*-phenylenediamine. The reaction of the ligand with Fe(III), Co(II) and Ni(II) salts in an 1:1 ratio yielded three complexes (**1**–**3**). Different analytical tools, like elemental analysis, ESI-MS, UV–Vis, FT-IR, NMR and EPR spectroscopy, then molar conductivity and magnetic susceptibility spectra, were used to elucidate the structure of the lig-and and complexes. Density functional theory calculation at the B3LYP/3--211G++/LANL2DZ level of the theory has been carried out to optimize the geometry of the ligand and complexes. The tetradentate ligand has coordinated to metals through ONNO donors affording octahedral geometry. Complexes were studied for their oxygen-binding activity and free radical scavenging acti-vities. Complexes **1** and **2**, which contain Fe(IIl) and Co(II), displayed rever-sible oxygen binding activity. On the other hand, complex **3** fails to show oxy-gen binding. The order of antioxidant activity is: **3** > **1** > **2** > **L**.

Keywords: oxygen binding study; thermodynamic parameters; FT-IR spectra; UV–Vis spectra.

INTRODUCTION

The discovery of reversible oxygenation of salicylaldimine cobalt complex by Tsumaki in 1938[1] has given considerable impetus to this objective. Since then, it has been inspiring synthetic chemists to prepare artificial respiratory pig-ment systems to imitate the natural ones in their activity. The proteins respon-sible for oxygen transportation and storage in mammalian cells, haemoglobin (Hb) and myoglobin (Mb), have often been used as examples of protein conform-

---

941

ation, dynamics and function.[2] The compounds called natural respiratory pigments can reversibly absorb molecular oxygen.[3] Naturally occurring oxygen carriers and storage proteins contain a transition metal ion to which O_2 can reversibly bind, typically iron (in the form of ferrous heme in proteins such as myoglobin and haemoglobin) or copper (hemocyanin). Many complexes of this type have been used as models to aid in understanding protein's function. Cobalt-sub–stituted oxymyoglobin (CoMbO$_2$) was also characterized, as well as synthetic analogues.[4] Cobalt(II) complexes of Schiff bases, porphyrins or phthalocyanines have been widely studied as models of oxygen carriers.[5]

Interestingly, four-coordinated Schiff base derivative and macrocyclic complexes of cobalt(II) are poor oxygen binders. In contrast, their corresponding five-coordinate cobalt complexes with heterocyclic as the cobalt(II) ligand readily bind oxygen reversibly under an ambient pressure of oxygen.[6] The reversible O_2 binding can also occur for dicobalt(II) systems based on alkoxido and phenolato-hinged dinucleating ligands. In these, both cobalt atoms are oxidized from Co(II) to Co(III) by the oxidative addition of dioxygen, thus facilitating the reduction of O_2 to peroxide rather than the highly reactive superoxide as is the case for the mononuclear systems and which are prone to irreversible self-annihilation reaction.[7] With the experience of Co(salen) and other complexes and their O_2 binding activity many complexes incorporating Co(II), Fe(III) and Ni(II) have been prepared with different tetradentate Schiff base in search of good oxygen--binding activity.[8] Presence of oxygen in the living system is an essential condition for the survival of the organism. Still, it is also associated with the generation of different free radicals in the system. The living systems have the inherent protective mechanism to disseminate and neutralize these radicals. However, sometimes due to a higher concentration of the free radicals in the body system, a life-threatening situation may occur. In this situation role of free radical scavenger known as antioxidants become more important.[9]

Therefore, in anticipation of good reactivity, oxygen-binding activity and effective antioxidant activity of the resulting complexes, we have prepared a tetradentate Schiff base by condensation of 2,4-dihydroxybenzaldehyde with *o*-phenylenediamine. The reaction of the ligand with Fe(III), Co(II) and Ni(II) leads to the synthesis of three novel complexes. Synthesized compounds were characterized by spectroscopy. In the absence of a single crystal, density functional theory (DFT) studies have been performed to optimize ligand and complexes' structure. A general scheme for the synthesis of ligand and complexes is given in Fig. 1.

EXPERIMENTAL

o-Phenylenediamine (Research Lab), 2,4-dihydroxybenzaldehyde (Sigma–Aldrich), anhydrous FeCl$_3$, CoCl$_2 \cdot$6H$_2$O, NiCl$_2 \cdot$6H$_2$O were purchased from E. Merck. Analytical reagent grade solvents were used. Conductivity measurements were carried out at 25 °C on an EI-
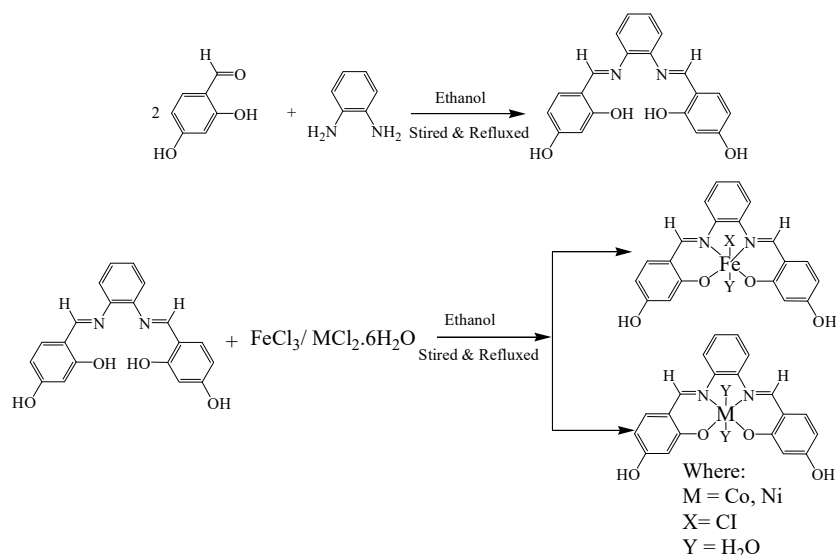
Fig. 1. General scheme for the synthesis of ligand **L** and complexes.

-181 conductivity bridge with a dipping type cell. ESI-MS spectra were recorded on Agilent-6520(QTOF) mass spectrometer. FT-IR spectra were recorded in KBr pellets on Shimadzu-8400 PC. Electronic absorption spectra were recorded with EI-2305, double beam spectrophotometer equipped with a PC. ^{1}H-NMR and ^{13}C-NMR spectra were recorded in DMSO-d_6 on Agilent-700-vnmrs 700. The metal contents were analyzed gravimetrically by the literature procedure. EPR spectra of the complexes were recorded at X-band (9.439 GHz) frequency in the EPR JEOL spectrometer.

*Synthesis of Schiff base ligand (7E)-N-benzylidene-2-styrylbenzenamine-1,2-diamine-2,4-dihydroxy-phenol (**L**)*

2,4-dihydroxybenzaldehyde (2.76 g, 0.010 mol) dissolved in 25 mL of ethanol was mixed with a solution of *o*-phenylenediamine (1.08 mL, 0.010 mol) in 25 mL of ethanol in a flat bottom flask, and the resulting mixture was stirred for 1 h. After that, the reaction mixture was kept under reflux for 8 h in an inert atmosphere. A pale yellow solid was obtained after cooling the mixture, which was filtered off, washed several times with methanol. The solid obtained was recrystallized from hot methanol to yield yellow crystals, dried over anhydrous calcium chloride in a desiccator under vacuum.

Synthesis of complexes

Ligand (**L**, 0.348 g, 0.0010 mol) was dissolved in 25 mL ethanol in a two neck flat bottom flask. FeCl$_3$ (0.161 g, 0.001 mol)/CoCl$_2$·6H$_2$O (0.237 g, 0.0010 mol)/NiCl$_2$·6H$_2$O (0.237 g, 0.0010 mol) dissolved in 25 mL ethanol was added to the above reaction mixture dropwise and stirred for 2 h. After that, the reaction mixture was refluxed for 9 h in an inert atmosphere. A red precipitate was obtained, filtered, recrystallized by 2:2:1 volume ratio of ethanol:methanol:acetone solvent mixture, and dried in a vacuum. Unfortunately, after several attempts, we did not find any crystal suitable for single-crystal XRD.

DFT Study

Density functional theory (DFT) was employed to achieve more insight into the molecular structure. It was carried out using the method of B3LYP with 6-311++G(d,p) basis set for all nonmetallic atoms and Los Alamos National Laboratory 2 double zeta (LANL2DZ) basic set for the central metal atoms in the gas phase.[11] Gaussian-09 software package was employed to carry out all the quantum chemical calculations.[12] Optimized structural parameter of the compounds, such as bond lengths and bond angles, were calculated with the molecule's atom numbering scheme. Several quantum chemical parameters have been calculated.[13] The FT-IR, ^{1}H-NMR and ^{13}C-NMR Chemical Shifts of the molecule were calculated by the gauge-independent atomic orbital (GIAO) method and compared with experimental results.

Oxygen binding study

A reversible oxygen-binding study of the synthesized complexes was done in the experimental setup described earlier.[14] In the second experiment, the most effective iron and cobalt complexes were studied further, and oxygen-binding ability was observed at different temperatures (273–303 K) in DMF.[15] The thermodynamics parameter such as ΔH^o and ΔS^o were calculated using Van't Hoff equation.[16,17]

Antioxidant activity

The free radical scavenging activity of the compounds was determined with the 2,2-diphenyl-1-picrylhydrazyl (DPPH) method. Four solutions of different micromolar concentrations of the compounds (0.002, 0.004, 0.006 and 0.008 μM) and standard ascorbic acid were prepared in ethanol. The volume of each test tube was adjusted to 1.0 mL by adding ethanol. DPPH was used as a control. After that, a 5 mL ethanolic solution of DPPH (0.1 μM) was added. The tubes were kept at ambient temperature for 30 min. The absorbance of test solutions and a blank solution of DPPH (2 mL) was measured at 517 nm. The decrease in the absorbance of DPPH was calculated comparative to the measured absorbance of the control.[18] Radical scavenging activity was calculated as:

$$\text{Radical scavenging activity, \%} = 100\frac{A_{\text{control}} - A_{\text{test}}}{A_{\text{control}}} \tag{1}$$

where A_{control} is absorbance of the control and A_{test} is absorbance of the test.

RESULTS AND DISCUSSION

Spectral characterization of complexes

Stoichiometries of the complexes conformed with elemental analyses data. Molar conductance (Λ_{m}) for complexes in 10^{-3} M concentration in DMSO was in the range 1–4 Ω^{-1} cm^2 mol^{-1}, indicative of their 1:1 electrolytic nature.[19] ESI-MS spectra of complexes exhibit several peaks. However, a pseudomolecular ion peak for [M+H$^+$] was present consistently in each case, which indicated the molecular mass. ESI-MS spectra of ligand **L** and complexes are shown in Figs. S-1 and S-2a–c of the Supplementary material to this paper, respectively.

In the FT-IR spectrum of complexes, the band observed at ~3207 cm^{-1}, assigned for –OH vibration in ligand completely vanished, and a new peak at lower frequency appeared at ~512 cm^{-1}, which was assigned to M–O.[20] The appearance of this peak indicates the bonding of metal with phenolic oxygen.

The band due to azomethine HC=N groups was shifted downwards by 1598 cm^{-1} in complexes, which confirms the coordination of azomethine nitrogen with metal. The coordination of azomethine nitrogen with metal was further ascertained by the appearance of a peak at a lower frequency at ~433 cm^{-1}, assigned to M–N vibration stretching.[21] Complexes also exhibit a band observed at ~2871 cm^{-1} attributed to the aromatic ring's C–H vibration. The vibrational band for C–O stretching was observed at ~1180 cm^{-1}.[22] The experimental (solid phase) and theoretical (gas phase) FT-IR spectra data of **L** and complex **2** is correlated in TABLE S-I of the Supplementary material.

The calculated IR vibrations were slightly shifted from experimental values. DFT calculations generally overestimate the frequencies and neglect the crystal packing effects. However, anharmonicity and incompleteness of the basis set and dynamic electronic correlation were also responsible for the above-stated deviations.[23] Therefore, we have derived scaling factors and applied them to get a satisfactory value. The scaling factor for **L** was determined as 1.012 ($R^2 = 0.999$) over a complete range of spectrum and that in complex **2,** it is 1.005 ($R^2 = 0.998$). In comparison, it was observed that in the theoretical spectra after scaling, the peaks for ν(C–H), ν(HC=N), ν(C–O)$_{sym}$, ν(C–C), ν(C–H), ν(O–H), ν(M–O) and ν(M–N) were observed with a very small deviation of 0.1 %. The experimental and theoretical FT-IR spectra of ligand **L** are shown in Figs. S-3 and S-4 of the Supplementary material. Similarly, the experimental and theoretical FT-IR spectrum of complex **2** is shown in Figs. S-5 and S-6. The FT-IR correlation curve for ligand **L** and complex **2** is shown in Fig. S-7. The experimental spectra of complexes **1** and **3** are shown in Figs. S-8 and S-9.

In the UV–Vis spectra of ligand **L**, an absorption band at 280 nm was assigned to the intra-ligand $\pi{\rightarrow}\pi^*$ transition, and a strong absorption band at 340 nm was ascribed to $n{\rightarrow}\pi^*$ transition associated with imine moiety. Fe(III) complexes exhibit a magnetic moment of ~5.54 BM as expected for the high spin case. The ground state of high spin octahedral Fe(III) complexes is $^6A_{1g}$. The electronic spectrum of this complex exhibits bands at 660, 540 and 340 nm assigned for the following transitions: $^6A_{1g}{\rightarrow}^4T_{1g}$, $^6A_{1g}{\rightarrow}^4T_{2g}$ and $^6A_{1g}{\rightarrow}^4T_{1g}$, ^4E_g, respectively, as expected for the iron(III) octahedral complexes. Co(II) complexes exhibit magnetic moments of ~4.59 BM due to the presence of three unpaired electron. The electronic spectrum of complexes exhibits bands at ~630, ~560 and ~390 nm assigned for the following transitions: $^4T_{1g}$ (F)$\rightarrow$$^4T_{2g}$ (P) (ν_1), $^4T_{1g}$ (F)$\rightarrow$$^4A_{2g}$ (F) (ν_2) and $^4T_{1g}$ (F)$\rightarrow$$^4T_{2g}$ (F) (ν_3), respectively. This transitions suggest an octahedral environment around the cobalt(II) ion.[24] Ni(II) complexes exhibit ~3.02 BM, indicating two unpaired electrons in Ni(II) ion consistent with octahedral geometry. A spectrum of the nickel(II) complex exhibits three bands at ~610, ~520 and ~360 nm corresponding to $^3A_{2g}{\rightarrow}^3T_{2g}$, $^3A_{2g}{\rightarrow}^3T_{1g}$ and $^3A_{2g}{\rightarrow}^3T_{1g}(P)$ transitions, respectively, which indicate an octa-

hedral geometry around nickel atom.[25] UV–Vis spectra of **L** and complexes are given in Figs. S-10 and S-11a–c of the Supplementary material.

^{1}H-NMR of **L** exhibits a signal at δ 8.81 ppm for two protons (numbered as 3 and 16) were attributed to two azomethine group present in the ligand. It is positive evidence for the Schiff base formation.[26] Two deshielded signals appeared at δ 13.18 and ~9.91 ppm for two protons each, were assigned for the phenolic-OH present at ortho (numbered as 40 and 41) and para-position (numbered as 39 and 42) to azomethine. A multiplet centred at δ 6.87 ppm for four protons were due to four phenylene proton atoms (numbered as 10, 11, 12 and 13). A double doublet centred at δ 7.56 ppm for two protons were assigned to the phenolic ring proton atoms present ortho to azomethine (numbered as 3 and 24). A multiplet centred at δ 7.37 ppm for two protons was attributed to phenolic ring proton atoms present meta to azomethine (numbered as 25 and 33). A singlet for two protons at δ 6.36 ppm was attributed to phenolic ring proton atoms present between two hydroxyl groups (numbered as 23 and 32). The ^{1}H-NMR spectrum of ligand **L** is shown in Fig. S-12. The GIAO method calculated the theoretical chemical shift values using TMS HF/6-31G(d) GIAO and TMS B3LYP/6--311+G(2d,p) GIAO level theory. The correlation coefficients of ^{1}H-NMR were determined as 0.978, as shown in Fig. S-13. For ligand **L** ^{1}H-NMR δ_{cal} 0.934, δ_{exp} + 0.327 (R^2 = 0.978). It was evident from the correlation graph that good correlation exists in theoretical and experimental δ values.

In the ^{13}C-NMR of ligand **L**, a strong signal at δ ~173.0 ppm was assigned for the presence of imine (>C=N–) carbon. The signal that appeared at δ ~166.0 ppm was attributed to the carbon linked with a hydroxyl group. All aromatic carbon of phenylene and phenolic moiety display signals between δ 116.00 and 162.00 ppm.[27] The ^{13}C-NMR spectrum of **L** is shown in Fig. S-14. The correlation coefficients of ^{13}C-NMR for **L** was determined as 0.942, as shown in Fig. S-15. For **L,** ^{13}C-NMR δ_{cal} 0.856, δ_{exp} + 22.68 (R^2 = 0.942). It was evident from the correlation graph that a good correlation exists in theoretical and experimental δ values. The DFT and ^{1}H-NMR and ^{13}C-NMR were correlated with the experimental and theoretical δ values. Data of **L** are displayed in TABLE S-II.

The EPR analysis of complexes **1–3** was performed at solid-state at room temperature (RT).[28] Spin-Hamiltonian parameters calculated for complex **1** at RT shows *g* values: $g_\perp \approx 2.408$, $g_\parallel \approx 2.086$ and $g_e \approx 2.009$. Spin-Hamiltonian parameters calculated for complex **2** at RT shows *g* values: $g_\perp \approx 2.554$, $g_\parallel \approx$ ≈ 2.148 and $g_e \approx 2.013$. Spin-Hamiltonian parameters calculated for complex **3** at RT shows *g* value: $g_\perp \approx 2.354$, $g_\parallel \approx 2.048$ and $g_e \approx 2.011$, suggesting that the unpaired electron resides in $d_{x^2-y^2}$ orbital and slightly distorted octahedral geometry of the complexes. The EPR spectra of complexes **1–3** are shown in Fig. S-16a–c.

Quantum chemical calculations

The Mulliken population analysis obtained the net atomic charges of ligand, **L** and complex **2**.[29] The Mulliken charge shows that in **L** maximum charge of +0.28944 is observed on C27 because C27 is flanked between three highly electronegative atoms. Electronegative atoms such as O, N, N and O exhibit highly negative charge due to the +I effect. O38 atoms from the hydroxyl group being highly shielded have a maximum negative Mulliken charge value of -0.62650, and azomethine-N have a charge of -0.27821. In complex **2,** maximum +*ve* charges of +0.326542 are observed on C27 since C27 is flanked between three highly electronegative atoms. Electronegative atoms such as O, N, N and O exhibit highly negative charge due to the +I effect. O41 atoms from the hydroxyl group being highly shielded have a maximum –*ve* Mulliken charge of -0.580976, and azomethine-N have a charge of -0.319319. The Mulliken charges of all complexes are listed in TABLE S-III.

The atomic charge distributions for the complex was calculated with the B3LYP/LanL2DZ//6–311++G* basis set. The highest and lowest negative charge to be found on complex **2** at N(2) (–0.47669 e) and O(37) (–0.74449 e). Thus the observed bond length of Co–N(14), 1.87956 Å and Co–O(35) 1.82787 Å are different. According to the NPA, the natural electron configuration of Co is: [core] 4s(0.26)3d(7.65)4p(0.51)4d(0.02). Thus, (17.99025) core electrons, (8.41330) valence electrons (on 4s, 3d and 4p atomic orbitals) and (0.02571) Rydberg electrons (mainly on 4p, 4d and 5p orbitals) give 26.42926 electrons. This value is consistent with the calculated natural charge on Co atom +0.57074 in complex **2**, which corresponds to the difference between 26.42926 e and the total number of electrons in the isolated cobalt atom 27 e. In addition, the atoms O(35), O(36), N(2) and N(14), have negative charge –0.63188, –0.61051, –0.47669 and –0.54181 e, respectively. The charges of the atoms in the ligand **L** and complex **2** are listed in TABLE S-IV.

The natural bond orbital (NBO) analysis of a representative complex **2** was carried out by the B3LYP/LANL2DZ level basis set.[30] As expected, the strongest donation occurs in the ligand **L**, which from the π(N2–C2) to π*(C6) antibonding orbital and has the energy of 157.60 kJ/mol. The interaction between the σ(C2–C5) and σ*(N2–C5) has the second-highest value of around 105.65 kJ/mol. These transitions give greater stabilization to the molecule. The hyper conjugative interactions of the σ and π electrons of selected C–C to anti– C–C bonds in the complex **2** are listed in TABLE S-V. The values of stabilization energies are in the range of 0.29–1.10 kJ/mol for σ→σ* transitions, 0.58-44.80 kJ/mol for π→π* transitions. The π→π* transitions have high resonance energies, such as C28-C29→C26-C27, C26-C27→C30-C31, C30-C31→C28-C29, C17 C18→ →C21-C22, C21-C22→C15-C20 and C15-C20→C21-C22, with the resonance energies 10.52, 10.50, 11.02, 11.10, 13.69 and 44.80 kJ/mol, respectively, that

lead to the stability of the complex. According to the n→σ* and n→π* interactions, the strongest interactions are due to LP(1)C1→σ*(C30–C31) 17.52, LP(1)N→σ*(O36–Co44) 28.00, LP (1)C19→σ*(C15–C20) 98.94, LP (1)C19→ →π*(C17–C18) 37.97, LP*(6)Co44→π*(N2–C5) 84.91, LP*(6)Co44→ →π*(C4–C5) 16.57, π(N2–C5)→LP*(4)Co(44) 21.22 kJ/mol.

The molecule's MEP surface was calculated by the B3LYP/LANL2DZ method with the 6-311++G(d,p) basis set. As it can be easily observed from the ligand **L** MEP map, the negative regions in MEP are related to the electronegative or electrophilic site. In contrast, the positive regions are related to the electropositive or nucleophilic site. This molecule has several possible sites for coordination. The negative regions are mainly over the oxygen atoms (deep red/yellow) on each of the O–H groups and nitrogen atoms of imine groups. The oxygen and carbon atoms bear the maximum region of positive charge, and the most positive regions (blue/green) are observed around the O–H groups as well as carbon atoms of imine groups. The colour codes of this map are in the ranges between –0.122 (deep red) and +0.122 a.u. (deep blue) in the ligand **L**. Similarly, in the complexes, the MEP map is between –0.113 and +0.113 a.u. for complex **1**, –8.512 and +8.512 a.u. for complex **2** and –9.163 and + 9.163 a.u. for complex **3**, respectively. The potential increases in the order: red < orange < yellow < < green < blue.[31] The MEP map of ligand **L** and comple**xes** are shown in Fig. S-17a–d.

FMOs analysis

The HOMO is the orbital that primarily acts as an electron donor, and the LUMO largely acts as the electron acceptor. The energy gap between HOMO and LUMO set apart the chemical stability of the molecule.[32] The FMOs of the energies of compounds are shown in TABLE S-VI. The energy differences between HOMO and LUMO for ligand **L** is 4.13035 eV while in complexes 3.04545, 3.54941 and 2.97987 eV, respectively. The HOMO and LUMO energy level diagrams of ligand **L** and complex**es** are shown in Fig. S-18a–d. The calculated energies of the HOMO and LUMO show that there is a very small energy gap (ΔE) in complex **3,** which may be responsible for its low kinetic stability, reflecting efficient electronic charge transfer interaction and high chemical reactivity, making the ligand strongly polarizable. It may lead to high free radical scavenging activity.

Bond parameters

The optimized bond lengths and bond angles of investigated compounds calculated by B3LYP/LANL2DZ methods with 6-311++G (d,p) basis set were listed in TABLEs S-VII and S-VIII following the atom numbering scheme as shown in Fig. 2a–d. The optimized geometrical parameters of ligand were compared with complexes. The optimized O–H bond length in ligand was 0.962 Å

which was diminished in complexes, and a new M–O bond is formed with a bond length of 1.800–1.828 Å. The calculated >C=N– bond distance in ligand was observed as ~1.293 Å, which shows an increase of 0.005–0.006 Å in the case of complexes. This increase in the bond distance is due to the transfer of double bond electron density towards metal and the decrease in the double bond character of C=N, which confirms the coordination of metal with azomethine-N. This elongation in M–N bond lengths caused a slight distortion from the regular octahedral geometry.
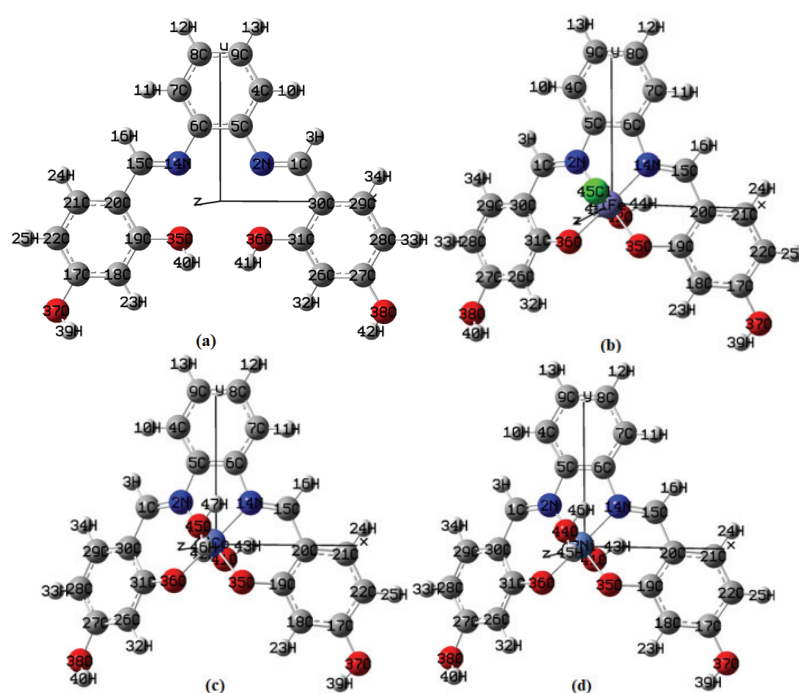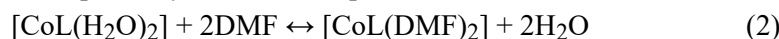

Fig. 2. DFT optimized structure of: a) ligand **L** and complexes: b) **1**, c) **2** and d) **3**.

Based on elemental analysis, electronic spectra, ESI-MS, FT-IR, ^{1}H-NMR, ^{13}C-NMR and DFT studies, optimized structures of the ligand **L** is suggested in Fig. 2a. Similarly, based on elemental analysis, molar conductance, electronic spectra, ESI-MS, FT-IR, EPR and DFT studies, optimized structures of the complexes are given in Fig. 2b–d.

Oxygen binding study

Complexes dissolved in DMF were explored for Oxygen binding study, and results are shown as spectra in Fig. 3. Absorbance change was noticed only in complexes **1** and **2** containing Fe (III) and Co (II) as a central metal ion. However, complex **3** exhibited no change in the absorbance; Ni (II) as a central metal.

It could be explained based on DFT optimization. It was observed in DFT optimized structure that Ni–O(H$_2$O) bonds are slightly smaller than other M–O(H$_2$O) bonds and probably more stable, which may be the reason for the non-participation of these complexes in oxygen binding activity. From the graph, it was observed that the prominent absorption at 360 nm in complex **1**, 390 nm in complex **2** diminished with time and seems to disappear in the presence of oxygen. Interestingly, at the same time, the absorption of broad bands between 440–650 nm attributable to d–d transitions becomes more pronounced. In cobalt complexes, the reaction that most probably occurs in the presence of O$_2$ is:

$$[CoL(H_2O)_2] + 2DMF \leftrightarrow [CoL(DMF)_2] + 2H_2O \qquad (2)$$

$$[CoL(DMF)_2] + O_2 \leftrightarrow [CoL(DMF)(O_2)] + DMF \qquad (3)$$

However, in the case of Fe (III) complex reaction appears to proceed in the following manner:

$$[FeL(H_2O)Cl] + DMF \leftrightarrow [FeL(DMF)Cl] + H_2O \qquad (4)$$

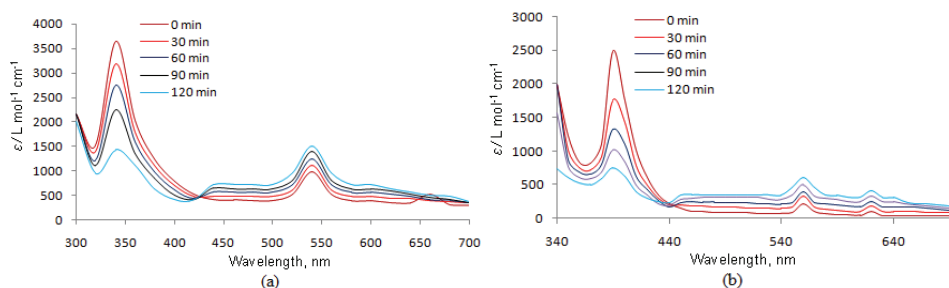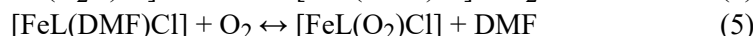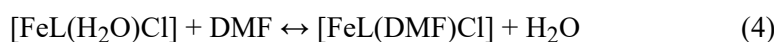$$[FeL(DMF)Cl] + O_2 \leftrightarrow [FeL(O_2)Cl] + DMF \qquad (5)$$

Fig. 3. UV–Vis spectra of oxygen binding study of complexes **1** (a) and **2** (b).

To understand the thermodynamics of oxygen binding reaction of complexes, the reaction was carried out at various temperatures and the oxygenation constant (K_{O_2}), which is calculated according to the relation below:

$$K_{O_2} = (CML(DMF)_{O_2}/CML(DMF))P_{O_2} \qquad (6)$$

The data clearly show that the oxygenation constant decreases with an increase in temperature, which indicates that the oxygen-binding ability of complexes decreases with rising temperature.[33] The oxygenation constants at different working temperatures are given in TABLE S-IX. The experimental values of K_{O_2}, at different temperatures, obey the Van't Hoff equation.[34] To determine the thermodynamic parameters, such as $\Delta H°$ and $\Delta S°$, the plot of ln K_{O_2} *vs.* 1000/T was drawn Fig. S-19:

$$\ln K_{O_2} = f(1/T) \qquad (7)$$

$$\ln K_{O_2} = -(\Delta H°/RT) + (\Delta S°/R) \qquad (8)$$

It was observed from TABLE S-IX that the enthalpy change of complex **1** is maximum negative. Negative enthalpy change is also an indicator of exothermic oxygenation reaction. The negative value of $\Delta H°$ and $\Delta S°$ for complexes **1** and **2** demonstrate that these complexes consist of a good oxygen-binding capacity.[35]

In vitro *antioxidant activity*

The results of the free radical scavenging activity of the compounds at different micromolar concentrations (0.002–0.008 μM) are shown in TABLE S-X. Ascorbic acid was used as a control to estimate the effectiveness of the tested compounds under the same conditions. The measured compounds have exhibited significant scavenging activity but lower than ascorbic acid. It has been observed that complex **3** exhibited higher antioxidant activity of 46.33–76.33 % in the given concentration range. It could be explained based on DFT, which calculates the lower energy gap (ΔE) for complex **3**. Due to the lower energy gap (ΔE),[36] complex **3** will be more reactive and can easily react with the free radicals to yield a more resonance stabilized complex species.

CONCLUSION

A Schiff base ligand (7*E*)-*N*-benzylidene-2-styrylbenzenamine1,2-diamine--2,4-dihydroxy-phenol (**L**) and its novel metal derivatives of Fe(III), Co(II) and Ni(II) were synthesized and characterized by spectroscopy. The spectral data has revealed that the Schiff base acts as a tetradentate ONNO donor ligand and coordinated through phenolic oxygen and azomethine nitrogen. In FT-IR and NMR, a quite good correlation has been observed in experimental and theoretical data. Several quantum chemical calculations have been performed to achieve better insight into molecular structure, and the geometry of complexes was optimized. The bond parameters, bond distance and bond angles are slightly distorted from octahedral geometry. In oxygen-binding experiment, **1** and **2** with Fe(III) and Co(II) exhibited good oxygen-binding capacity; however, **3** with Ni(II) ion is inactive probably due to greater stability of Ni–O(H$_2$O) bonds. The negative values of $\Delta H°$ and $\Delta S°$ for **1** and **2** demonstrated that oxygenation reaction is thermodynamically favored for these complexes. The decrease in oxygenation constant with temperature indicates that the oxygen-binding ability of complexes decreases with an increase in temperature. In the antioxidant activity experiment, complex **3** displayed more antioxidant activity than **1**, **2** and **L**, probably due to lower ΔE.

SUPPLEMENTARY MATERIAL

Additional data and information are available electronically at the pages of journal website: https://www.shd-pub.org.rs/index.php/JSCS/article/view/10208, or from the corresponding author on request.

И З В О Д

СИНТЕЗА, СПЕКТРОСКОПСКА КАРАКТЕРИЗАЦИЈА, DFT ПРОРАЧУНИ, ВЕЗИВАЊЕ КИСЕОНИКА И АНТИОКСИДАТИВНА АКТИВНОСТ КОМПЛЕКСА Fe(III), Co(II) И Ni(II) СА ONNO-ТЕТРАДЕНТАТНОМ ШИФОВОМ БАЗОМ КАО ЛИГАНДОМ

SATYENDRA N. SHUKLA, PRATIKSHA GAUR, MOHAN L. RAIDAS и SANJAY S. BAGRI

Coordination Chemistry Research Lab, Department of Chemistry, Govt. Science College, Jabalpur (M.P.), India

Кондензационом реакцијом између 2,4-дихидроксибензалдехида и *o*-фенилендиамина добијена је Шифова база (7*E*)-*N*-бензилиден-2-стирилбензенамин-1,2-диамин- -2,4-дихирдоксифенол (**L**), која је затим у реакцаији са Fe(III), Co(II) и Ni(II) солима (молски однос 1:1) употребљена као лиганд за синтезу одговарајућих комплекса (**1**–**3**). Различите аналитичке технике, као што су елементална анализа, ESI-MS, UV–Vis, FT-IR, NMR и EPR спектроскопија, а затим метода мерења моларне и магнетне проводљивости, употребљене су за структурну карактеризацију лиганда и одговарајућих комплекса метала. Применом DFT методе на бази B3LYP/3-211G^{++}/LANL2DZ теоријских прорачуна оптимизована је геометрија лиганда и комплекса метала. Нађено је да је лиганд **L** преко ONNO донорских атома тетрадентатно координован за јоне метала при чему настају комплекси октаедарске геометрије. Испитивана је способност комплекса за везивање кисеоника и слободних радикала. Комплекси Fe(III) и Co(II) (**1** и **2**) су показали реверзибилну способност везивања кисеоника. Супротно томе, комплекс **3** није показао способност везивања кисеоника. Антиоксидативна активност испитиваних једињења мењала се у низу **3** > **1** > **2** > **L**.

(Примљено 30. децембра 2020, ревидирано 14. марта, прихваћено 7. априла 2021)

REFERENCES

1. V. Tsumaki, *Bull. Chem. Soc. Jpn.* **13** (1938) 262 (https://dx.doi.org/10.1246/bcsj.13.252)
2. M. F. Perutz, *Trends Biochem. Sci.* **14** (1990) 42 (https://dx.doi.org/10.1016/0968-0004(89)90039-x)
3. M. Wirstam, S. J. Lippard, R. A. Friesner, *J. Am. Chem. Soc.* **13** (2003) 3980 (https://dx.doi.org/10.1021/ja017692r)
4. M. S. Vad, F. B. Johansson, R. K. S. Egdal, J. E. McGrady, S. M. Novikov, S. I. Bozhevolnyi, A. D. Bonda, *Dalton Trans.* **42** (2013) 9921 (https://dx.doi.org/10.1039/c3dt50617g)
5. B. M. Hoffman, D. H. Petering, *Proc. Natl. Acad. Sci. USA* **67** (1970) 627 (https://dx.doi.org/10.1073/pnas.67.2.637)
6. J. H. Bowen, N. V. Shokhirev, A. M. Raitsimring, D. H. Buttlaire, F. A. Walker, *J. Phys. Chem., B* **101** (1997) 8683 (https://dx.doi.org/10.1021/jp9711306)
7. W. R. Scheidt, J. L. Hoard, *J. Am. Chem. Soc.* **95** (1973) 8281 (https://dx.doi.org/10.1021/ja00806a013)

8. A. A. A. Emara, A. M. Ali, A. F. El-Asmy, E. M. Ragab, *J. Saudi Chem. Soc.* **18** (2011) 762 (https://dx.doi.org/10.1016/j.jscs.2011.08.002)
9. L. Liu, M. S. Alam, D. U. Lee, *Bull. Korean Chem. Soc.* **33** (2012) 3361 (http://dx.doi.org/10.5012/bkcs.2012.33.10.3361)
10. G. H. Jeffery, J. Bassett, J. Mendham, R. C. Denney, *Vogel's Textbook of Quantitative Inorganic Analysis*, 5th ed., John Wiley & Sons, Inc., New York, 1989
11. M. Montazerozohori, S.A. Musavi, A. Masoudias, A. Hojjati, A. Assoud, *Spectrochim. Acta, A* **147** (2015) 139 (http://dx.doi.org/10.1016/j.saa.2015.03.028)
12. *Gaussian-09 software package*, Gaussian Inc. Wallingford, CT, 2009
13. M. Dehestani, L. Zeidabadinejad, *J. Serb. Chem. Soc.* **80** (2015) 1008 (https://dx.doi.org/10.2298/JSC150224027Z)
14. S. N. Shukla, P. Gaur, M. L. Raidas, B. Chaurasia, *J. Mol. Struc.* **1202** (2020) 127362 (https://dx.doi.org/10.1016/j.molstruc.2019.127362)
15. A. Huber, L. Müller, H. Elias, R. Klement, M. Valko, *Euro. J. Inorg. Chem.* **8** (2005) 1459 (https://dx.doi.org/10.1002/ejic.200400888)
16. T. J. Beugelsdijk, R. S. Drago, *J. Am. Chem. Soc.* **97** (1975) 6466 (https://dx.doi.org/10.1021/ja00855a028)
17. N. J. Rose, R. S. Drago, *J. Am. Chem. Soc*. **81** (1959) 6138 (https://dx.doi.org/10.1021/ja01532a009)
18. M. Kumar, T. Padmini, K. Ponnuvel, *J. Saudi Chem. Soc.* **21** (2017) 322 (https://dx.doi.org/10.1016/j.jscs.2014.03.006)
19. W. J. Gear, *J. Coord. Chem. Rev.* **7** (1971) 81(https://dx.doi.org/10.1016/S0010-8545(00)80009-0)
20. S. N. Shukla, P. Gaur, P. Vaidya, B. Chaurasia, S. Jhariya, *J. Coord. Chem.* **71** (2018) 3912 (https://dx.doi.org/10.1080/00958972.2018.1536267)
21. S. N. Shukla, P. Gaur, S. Jhariya, B. Chaurasia, P. Vaidya, M. Azam, *J. Coord. Chem*. **72** (2019) 664 (https://dx.doi.org/10.1080/00958972.2019.1572885)
22. N. Ignjatović, S. Vranješ, Ž. Mitić, D. Janković, D. Uskoković, *J. Mat. Sci. Eng., C* **43** (2014) 439 (https://dx.doi.org/10.1016/j.msec.2014.07.046)
23. A. P. Scott, L. Radom, *J. Phys. Chem.* **100** (1996) 16502 (https://dx.doi.org/10.1021/jp960976r)
24. S. Chandra, L. K. Gupta, *Trans. Metal Chem.* **32** (2007) 558 (https://dx.doi.org/10.1007/s11243-007-0201-y)
25. F. A. Cotton, G. Wilkinson, C. A. Murillo, M. Bochmann, *Advances in Inorganic Chemistry*, Sixth ed., Wiley, New York, 1999
26. R. Mehrotra, S. N. Shukla, P. Gaur, *J. Coord. Chem.* **65** (2012) 176 (https://dx.doi.org/10.1080/00958972.2011.645814)
27. R. M. Silverstein, F. X. Webster, D. J. Kiemle, D. L. Bryce, *Spectr. Ident. Org. Com.* **1991** (1998) 226
28. P. Pietrzyk, M. Srebro, M. Radon, Z. Sojka, A. Michalak, *J. Phys. Chem., A* **115** (2011) 2316 (https://dx.doi.org/10.1021/jp109524t)
29. T. Bardakçi, M. Kumru, A. Altun, *J. Mol. Struct.* **1116** (2016) 292 (https://dx.doi.org/10.1016/j.molstruc.2016.03.023)
30. S. Sebastian, N. Sundaraganesan, *Spectrochim Acta, A* **75**(2010) 941 (https://dx.doi.org/10.1016/j.saa.2009.11.030)
31. I. Rajaei, S. N. Mirsattari, *Polyhedron* **112** (2015) 479 (https://doi.org/10.1016/j.poly.2015.10.019)

32. J. M. Mir, D. K. Rajak, R. C. Maurya, *J. Coord. Chem.* **70** (2017) 3199 (https://dx.doi.org/10.1080/00958972.2017.1374381)

33. M. R. Anneser, S. Haslinger, A. Pöthig, M. Cokoja, V. D'Elia, M. P. Högerl, J. M. Basset, F. E Kühn, *Dalton Trans.* **45** (2016) 6449 (https://dx.doi.org/10.1039/c6dt00538a)

34. M. Pająk, M. Woźniczka, A. Vogt, A. Kufelnicki, *Chem. Central J.* **11** (2017) 90 (https://dx.doi.org/10.1186/s13065-017-0319-8)

35. A. Pui, *Croat. Chem. Acta* **75** (2002) 165

36. M. S. Alam, D-U Lee, *Bull. Korean Chem. Soc.* **36** (2015) 682 (https://onlinelibrary.wiley.com/doi/full/10.1002/bkcs.10132).